Materials Advances

ROYAL SOCIETY OF CHEMISTRY

PAPER

View Article Online
View Journal | View Issue

Cite this: *Mater. Adv.*, 2025, 6, 1695

Mass transfer kinetics of Cr(VI) adsorption on a green mussel shell-polyethersulfone membrane

Mohamad Ali Fulazzaky, *[a] Nur Atikah Abdul Salim,[bc] Mohd Hafiz Puteh,[cd] Tiffany Messer,[e] Mohd Hafiz Dzarfan Othman,[d] Ahmad Fauzi Ismail,[d] Juhana Jaafar[d] and Mukhlis A. Rahman[d]

Received 23rd October 2024,
Accepted 20th January 2025

DOI: 10.1039/d4ma01068j

rsc.li/materials-advances

Cr(VI) is toxic to human health and aquatic life, requiring removal from contaminated water. Green mussel shells incorporated into a polyethersulfone (GMSPES) membrane were designed to create a flat sheet adsorptive membrane crossflow treatment permeator (FSAMCFTP) to remove Cr(VI) from a synthetic solution (SS). The physicochemical properties of the GMSPES membrane were verified using a scanning electron microscope, atomic force microscope, and water contact angle goniometer. The adsorption capacities of GMSPES0.5, GMSPES1.0 and GMSPES1.5 were found to be as high as 13.41, 15.24 and 10.84 mg g^{-1}, respectively. The numerical simulation of data using generalized Fulazzaky equations enabled the prediction of the mechanisms and kinetics of external, internal and global mass transfers for the adsorption of Cr(VI) on the GMSPES membrane. Comparison of external and internal mass transfers facilitated the determination of mass transfer resistance, with the internal mass transfer rate beginning at 0.16 h, while the external mass transfer rate dominated for 3.00 h of the experiment. The verification of Cr(VI) adsorption by the GMSPES membrane with different GMS/PES ratios provides a comprehensive understanding of the FSAMCFTP process, contributing to the advancement of adsorptive membrane technology.

1. Introduction

The rapid industrialization and economic development of an area stimulated by the industrial applications of textile, manufactured leather, electropainting, chemical manufacturing, printing, dyeing, and metallurgy have resulted in the upsurge of Cr(VI) discharge in water.[1] The use of Cr(VI) is essential for tanning high-quality leather, production of pigments, manufacturing of stainless steel, and electroplating.[2,3] The presence of Cr(VI) in water is primarily caused by biomagnification, which negatively impacts human health through ingestion *via* respiratory inhalation, the digestive tract and/or skin contact. Exposure may lead to lung cancer, kidney damage and dermatitis.[4–6] Stringent effluent water quality standards to regulate the concentrations of Cr(VI) have been put forth by several countries to allow treated wastewater to be discharged into water bodies. The Bureau of Indian Industrial Effluent Standard has set a limit of <3.0 mg L^{-1} for Cr(VI) in treated wastewater,[7] while the Government of Japan requires the concentration of Cr(VI) in an effluent to be <0.5 mg L^{-1}.[8] The United States Environmental Protection Agency limits the discharge of Cr(VI) from industrial effluents to a concentration of 0.05 mg L^{-1}.[9] According to the European Union Directive, the permissible Cr(VI) concentration limits are in the range of 0.05–1.0 mg L^{-1} for treated industrial wastewater discharged into oceans, lakes and rivers and <1.0 mg L^{-1} for releasing into other aquatic environments.[10] The concentration limit for Cr(VI) enacted by the Malaysian Environmental Laws is recommended to be <0.05 mg L^{-1} to allow the release of industrial effluents into surface water.[11]

Excessive amounts of Cr(VI) in discharged water can be removed *via* various methods, including coagulation, electrochemical treatment, ion exchange, and adsorption.[2] The coagulation method requires expensive chemicals and thus is often not an economically viable option to remove Cr(VI) from contaminated water.[9] Electrochemical treatment offers an efficient method for removing Cr(VI) from industrial wastewater but requires high electricity consumption.[12] Using ion

[a] *Department of Environmental Science, Faculty of Engineering and Science, Universitas Ibn Khaldun Bogor, Jalan Sholeh Iskandar, Kedungbadak, Bogor 16162, Indonesia. E-mail: mohamad.ali.fulazzaky@uika-bogor.ac.id, fulazzaky@gmail.com*
[b] *School of Occupational, Safety & Health, Netherlands Maritime University College, 80000 NMUC, Johor Bahru, Johor, Malaysia*
[c] *Department of Water and Environmental Engineering, Faculty of Civil Engineering, Universiti Teknologi Malaysia, 81310 UTM, Skudai, Johor, Malaysia*
[d] *Advanced Membrane Technology Research Centre (AMTEC), Universiti Teknologi Malaysia, 81310 UTM, Skudai, Johor, Malaysia*
[e] *Biosystems and Agricultural Engineering, University of Kentucky, Lexington, KY 40506, USA*

exchange technique to remove Cr(VI) from contaminated water is associated with a high operating cost of the electrocoagulation system applied to the treatment of industrial wastewater.[6] Therefore, the adsorption process to remove Cr(VI) from contaminated water must have the following features: the simplicity of design and ease of operation associated with a low cost and less space requirement.[13] Utilizing agricultural waste-based materials (*e.g.*, rice husk, waste tea, walnut shell) and aquacultural waste-based materials (*e.g.*, crab shell, oyster shell, mussel shell) as low-cost natural adsorbents are of interest to remove the heavy metals from contaminated water. Using mussel shells wasted in vast quantities in the environment without an economic value is beneficial for removing dyes and heavy metals from wastewater.[14] However, the application of adsorption processes suffers drawbacks, such as small capacity, particle agglomeration and scaling to industrial wastewater.[15] Therefore, applying an adsorptive membrane to combine the technological advantages of membrane separation and adsorption by considering the permeability, selectivity, water flux and rejection rate is of interest in various environmental applications of wastewater treatment technology.[16]

Classification of the adsorptive membranes is based on the polymer and adsorbent. Various types of adsorbents, such as metals and metal oxides, carbon sinks, and natural sources, have been used to create adsorptive membranes. 3 wt.% nickel–iron oxide ($NiFe_2O_4$) nanoparticles incorporated in the hollow fiber membrane were used for the adsorption of Pb, Cu, Zn, Cd, Cr and Ni from aqueous solutions and have the adsorption capacity of 52, 42, 35, 24, 18, and 17.5 mg g^{-1}, respectively.[17] The nano-textured membranes incorporating bio-adsorbents of soy protein, oats, lignin, sodium alginate, and chitosan have an adsorption capacity for Pb ranging from 2 to 45 mg g^{-1}, depending on the type of the biopolymer.[18] The incorporation of biomaterials into adsorptive membranes is a promising technology of interest to remove heavy metals and dyes because of the high permeability, antifouling properties, and mechanical reinforcement effect of the adsorptive membrane.[19] The use of chitosan/polyethylene oxide/activated carbon nanofibrous membranes for the removal of Cu(II), Zn(II) and Pb(II) from aqueous solutions also resulted in adsorption capacities of 195.3, 186.2, and 176.9 mg g^{-1}, respectively.[20]

The choice of green mussel (*Perna viridis*) shells (GMS) as a promising potential natural adsorbent could be due to the presence of calcium oxide on the surface, which is favorable for replacing Ca^{2+} cations by Cr^{6+} cations, resulting in the adsorption of Cr(VI) ions from aqueous solutions.[21,22] A previous experiment using the incorporation of GMS with polyethersulfone (PES) called the GMSPES membrane, with the GMS/PES ratios of 0.0, 2.0 and 2.2, was referred to design a flat sheet adsorptive membrane crossflow treatment permeator (FSAMCFTP). This experiment was of interest to study the removal of Cr(VI) from synthetic solutions (SS), showing that the adsorption capacity of 3.2 mg g^{-1} for a GMS/PES ratio of 2.0 was higher compared to 1.45 mg g^{-1} for a GMS/PES ratio of 2.2.[23] Therefore, the application of the GMSPES membranes with the GMS/PES ratios of below 2.0 for sequestrating Cr(VI) from SS needs to be verified to gain a comprehensive insight into the behavioral mechanisms and mass transfer kinetics of Cr(VI) adsorption. The originality of this study was the creation of the FSAMCFTP with the GMS/PES ratios of 0.0, 0.5, 1.0 and 1.5 for sequestering Cr(VI) from SS, which was a continuation of a previous study.[23] To our knowledge, there is very limited literature regarding the use of GMS as an adsorbent for the development of adsorptive membranes, while the mass transfer kinetics of Cr(VI) adsorbed into the GMSPES membrane remains ambiguous. The limitation of this study was that it only focused on the numerical simulation of data using generalized Fulazzaky (GF) equations to predict the behavioral mechanisms and mass transfer kinetics of Cr(VI) adsorption without comparing it with other kinetic models. Therefore, the objectives of this study were: (1) to create a GMSPES membrane designed in the form of FSAMCFTP for removing Cr(VI) from SS and (2) to numerically simulate the experimental data using a series of GF equations, which will enable the prediction of the mechanisms and mass transfer kinetics and permit the determination of the mass transfer resistance (MTR) for the adsorption of Cr(VI) into the GMSPES membranes from SS.

2. Materials and methods

2.1. Chemicals and Cr(VI) synthetic solution

This study used the PES of Radal A300 as the main component of the adsorptive membrane and *N*-methyl-pyrrolidone (NMP) as the solvent to synthesize the GMSPES membrane. An inorganic chemical reagent of potassium dichromate ($K_2Cr_2O_7$) was used to produce the SS containing Cr(VI) ions. The PES polymer was obtained from Amoco Chemicals Sdn. Bhd., Pahang, Malaysia. NMP and $K_2Cr_2O_7$ were purchased from Merck Sdn. Bhd., Selangor, Malaysia. All chemicals and reagents used for this experiment were of analytical grade. SS was prepared by dissolving 294.19 mg of $K_2Cr_2O_7$ into 1.0 L of distilled water (DW), which resulted in a stock solution with 100 mg L^{-1} of Cr(VI). Then, 400 mL of stock SS was diluted into 1.0 L of DW to obtain a Cr(VI) concentration of 40 mg L^{-1} for the experiments of the FSAMCFTP process with different GMS/PES ratios of 0.0, 0.5, 1.0 and 1.5.

2.2. Preparation of the GMS adsorbent

For this study, approximately 1.5 kg of the GMS sample, which was collected from the waste disposal of Kampung Pasir Puteh at Pasir Gudang of Johor state – Malaysia, was used to prepare the GMS adsorbent. The GMS sample was cleaned to remove the impurities by washing several times with tap water (TW) and then dried in an oven at 30 °C for 24 h to evaporate the water. The dried GMS sample was crushed by a hammer, which resulted in a granular GMS material, and then sieved through a sieve fraction, which resulted in an average size of 0.52 mm. The granular GMS material as an adsorbent was then incorporated with PES to synthesize the GMSPES membrane for the adsorption of Cr(VI) from SS by designing an experiment for the FSAMCFTP process.

2.3. Synthesis of the GMSPES membrane

The flat sheet GMSPES membranes were synthesized according to the phase-inversion method[24,25] as part of the FSAMCFTP process. Firstly, the polymeric GMSPES dope solution was prepared by mixing GMS with NMP and then stirred with a magnetic stirrer (model S131435, Barnstead, United States) at 60 °C for 4 h and then PES was added into the dope solution and then homogenized stirring with a speed of 500 rpm at 60 °C for 8 h. Finally, the polymeric GMSPES dope solution was sonicated at 60 °C for 24 h to synthesize a homogenous GMSPES dope solution. The viscosity of the homogenous GMSPES dope solution was determined using the DV1 digital viscometer (Brookfield, United States) for different GMS/PES ratios (see Table 1).

The procedural fabrication of the GMSPES membrane was based on four steps: (1) the polymeric dope solution of GMSPES was evenly cast onto a flat glass plate using a casting glass rod to form the film with a thickness of around 250 μm, (2) immersion of the cast film was performed in a container containing TW at room temperature for 10 min to induce a phase-inversion, (3) the formed flat sheet GMSPES membrane was immersed into another container containing TW for 24 h for removing any residual NMP solvent, and (4) the flat sheet GMSPES membrane was dried in ambient air for 8 h to evaporate the moisture content. The composition and viscosity of the GMSPES membrane with different GMS/PES ratios are depicted in Table 1.

2.4. Characterization of the GMS adsorbent and GMSPES membrane

2.4.1. Chemical and physical characterizations of the GMS adsorbent. Analysis of the oxide compositions (in %) of the GMS adsorbent was performed using the energy dispersive X-ray fluorescence (EDXRF) spectrometer (Rigaku, Sendagaya, Shibuya-Ku, Tokyo, Japan). The determination of the Brunauer, Emmett and Teller (BET) surface area for the GMS adsorbent was carried out according to the multiple-point method using the Surfer Analyzer of the Thermo Scientific Flash 2000 Elemental Analyzer (Thermo Scientific Inc., Milan, Italy).

2.4.2. Physical characterizations of the GMSPES membrane. The surface and cross-sectional features of the GMSPES membranes were interpreted from the scanning electron microscopy (SEM) images (model TM3000, Hitachi, Japan). The GMSPES membrane sample was immersed in liquid nitrogen and then split using an appropriate spatula to gain a clear cross-sectional image of the GMSPES membrane. The GMSPES sample was passed through a sputter coater (Model SC502, Quorum Technologies, Lewes BN8 6BN, United Kingdom) and a sputter-platinum film was prepared to allow the electrons to interact with atoms within the GMSPES membrane.

The GMSPES surface roughness was determined using an atomic force microscope (AFM, SPA-300HV AFM, Seiko Instruments, Chiba, Japan). All the GMSPES membrane samples had a square size of 1.0 cm × 1.0 cm and were analyzed using a scan area of 5 μm × 5 μm to obtain the surface roughness value (R_a). The water contact angle (WCA) of the GMSPES membrane sample was analyzed using the contact angle goniometer (Model OCA15plus, DataPhysics Instruments GmbH, Filderstadt, Germany) according to the sessile drop method to gain insight into the hydrophobic or hydrophilic surface property of the GMSPES membrane. Therefore, 1.0 μL of deionized water was injected using the motor-driven micro syringe in nine different areas on the dry surface of the GMSPES membrane to obtain the average value of WCA.

The porous GMSPES membrane had an effective area of 25.0 cm^2 calculated according to the gravity method rather than *via* contact angle measurement[26] by submersing it into TW. The GMSPES membrane sample was weighted before and after immersion in TW for 24 h. The porosity of the GMSPES membrane was calculated using the equation:

$$P = \frac{W_a - W_b}{D_w \times S \times L} \quad (1)$$

P is the porosity of the GMSPES membrane, W_a (g) and W_b (g) are the weights of the wet and dried membranes, respectively, D_w (g cm^{-3}) is the water density at room temperature, S (cm^2) is the membrane surface area, and L (cm) is the wet membrane thickness.

The pure water flux (PWF) of the GMSPES membrane was calculated using the steady-state measurement from the quantity of water permeated into the flat sheet of the GMSPES membrane. An effective surface area of 0.00238 m^2 at 1.0 bar for 20 min was determined. The PWF for the GMSPES membrane sample was calculated using the equation:

$$J = \frac{V}{A \times t} \quad (2)$$

J (L m^{-2} h^{-1}) is the pure water flux in the GMSPES membrane, V (L) is the volume of the permeate collected during the experiment at time t of the experiment, A (m^2) is the effective surface area of the GMSPES membrane, and t is the time of the experiment (h).

Table 1 Composition and viscosity of the GMSPES membrane

Membrane	GMS/PES ratio	GMS (g) (wt%)	PES (g)	NMP (g)	Viscosity (Cp)
GMSPES0.0	0.0	0	20	80	393
GMSPES0.5	0.5	10	20	70	785
GMSPES1.0	1.0	20	20	60	2350
GMSPES1.5	1.5	30	20	50	6925

2.5. Experimental setup and operational procedure

This study used the laboratory-scale FSAMCFTP process consisting of a 1.0-L feed container, booster pump, pressure gauge, valve, membrane module with a 5.5-cm inner diameter, and 1.0-L permeate container, as shown in Fig. 1. The cost for the production of the laboratory-scale FSAMCFTP system consisting of the materials and equipment, preparation, and installation was 1000 USD. The GMSPES membrane, with an effective surface area of 0.00238 m^2, was placed in a stainless steel

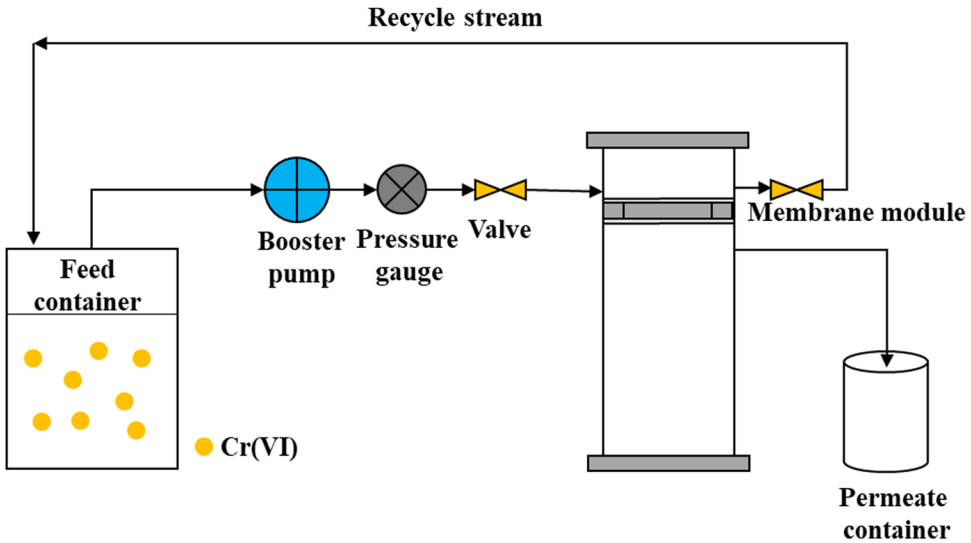

Fig. 1 Schematic of the FSAMCFTS process used to run the experiment.

membrane module to adsorb Cr(VI) from SS. The feeding of SS with a Cr(VI) concentration of 40 mg L^{-1} was performed at a constant flow rate of 0.096 L h^{-1} from the feed container toward the FSAMCFTP, one part passing through the GMSPES membrane to flow into the permeate container and another part recycling through the flexible plastic pipe into the feed container. The operating pressure and temperature of the FSAMCFTP process were kept constant at 1.0 bar and 25 °C, respectively, during the 3.5 h experiment to ensure the saturation of the GMS adsorbent. The Cr(VI) concentration was analyzed using the 1,5-diphenylcarbohydrazide method[27] in a UV-Vis Spectrophotometer (HACH DR 6000, Colorado, United States). The accumulative volume of the treated SS flowing into the permeate container was monitored at specific time intervals. The performance of the F SAMCFTP process to remove Cr(VI) from SS was analyzed by monitoring Cr(VI) concentrations at the inlet and outlet after passing through the GMSPES membrane. The dimensions and operating conditions for the experiments for the FSAMCFTP process are listed in Table 2 and were conducted using four membranes: GMSPES0.0, GMSPES0.5, GMSPES1.0 and GMSPES1.5, with the GMS/PES ratios of 0.0, 0.5, 1.0 and 1.5, respectively (see Table 1).

2.6. Numerical simulation

2.6.1. Calculation of the removal efficiency and adsorption capacity. The performance of the FSAMCFTP process was calculated based on the Cr(VI) concentrations monitored before and after passing through the GMSPES membrane for 3.5 h of the experiment. The removal efficiency of Cr(VI) adsorbed into the GMSPES membrane was determined using the equation:

$$E = \frac{C_o - C_s}{C_o} \times 100\% \quad (3)$$

E is the performance of the FSAMCFTP process to adsorb Cr(VI) from SS (%), C_o is the Cr(VI) concentration in the feed container (mg L^{-1}), and C_s is the Cr(VI) concentration in the permeate container (mg L^{-1}).

The adsorption capacity of the GMSPES membrane designed to form FSAMCFTP for a given Cr(VI) concentration and flow rate was calculated using the equation:

$$q = \frac{Q \times (C_o - C_s) \times t}{m} \quad (4)$$

q is the cumulative amount of Cr(VI) adsorbed into the GMSPES membrane (mg g^{-1}), Q is the flow rate of SS (L h^{-1}), C_o is the Cr(VI) concentration in the feed container (mg L^{-1}), C_s is the Cr(VI) concentration in the permeate container (mg L^{-1}), t is the time of the experiment (h), and m is the mass of GMS incorporated into the GMSPES membrane (g).

2.6.2. Numerical simulation by the generalized Fulazzaky equations. The cumulative amount of Cr(VI) adsorbed into the GMSPES membrane is calculated using the equation:[28]

$$q = \int_0^V \frac{(C_o - C_s)\mathrm{d}V}{m} \quad (5)$$

q is the cumulative amount of Cr(VI) adsorbed into the GMSPES membrane (mg g^{-1}), C_o is the Cr(VI) concentration in the feed container (mg L^{-1}), C_s is the Cr(VI) concentration in the permeate container (mg L^{-1}), V is the effective volume of the treated SS (L), and m is the mass of GMS incorporated into the GMSPES membrane (g).

The expanding application of the GF equations, which were empirically developed based on the Fulazzaky equations[29,30] to

Table 2 Dimensions and operating conditions for the FSAMCFTP process

Parameter	Unit	Value
Size of GMS adsorbent	mm	0.52
Internal diameter of the GMSPES membrane	cm	5.5
Height of the GMSPES membrane	cm	0.3
Hydraulic retention time	h	0.07
Flow rate	L h^{-1}	0.096
Pressure	bar	1.0

have a wider implication in the determination of mass transfer processes, enabled the prediction of the behavioral mechanisms and mass transfer kinetics of the adsorption, biosorption, decolorization, and biodegradation. The GF equations were recently used for the prediction of the behavioral mechanisms and mass transfer kinetics for the adsorption of p hosphate onto the waste mussel shell applied in a hybrid plug-flow column reactor,[31] biosorption of organic matter removed from palm oil mill effluent by developing biomass under anaerobic environment applied in a stirred cylinder batch reactor,[30] decolorization of mixed azo dyes in the presence of magnetic-activated carbon in the formation of aerobic granular sludge applied in a sequencing batch reactor,[32] and biodegradation of polyethylene mediated by bacterial-fungal consortium applied in a rectangular reactor.[33] The purpose of this work was to obtain a comprehensive understanding of the application of the GF equations to predict the mechanisms and kinetics of the external, internal and global mass transfers for the adsorption of Cr(VI) from SS into the GMSPES membrane, following a previous experiment of the FSAMCFTP process[23] by varying the GMS/PES ratios of 0.0, 0.5, 1.0 and 1.5. The numerical simulation of data was done using a series of the GF equations[34] below:

$$\ln\left(\frac{C_o}{C_s}\right) = [k_L a]_g \times e^{-\beta \times \ln(q)} \times t \quad (6)$$

By deducing eqn (6), the following linear equation[34] can be written:

$$\ln(q) = \frac{1}{\beta} \times \ln(t) + B \quad (7)$$

with

$$B = \frac{\ln\left([k_L a]_g\right) - \ln\left\{\ln\left(\frac{C_o}{C_s}\right)\right\}}{\beta} \quad (8)$$

The correlation of the external (film) mass transfer (EMT) factor with the global mass transfer (GMT) factor can be written using the mathematical formula:[34]

$$[k_L a]_f = [k_L a]_g \times e^{-\beta \times \ln(q)} \quad (9)$$

The mathematical equation of correlating internal (porous diffusion) mass transfer (IMT) factor with the GMT factor and the EMT factor can be written as:[34]

$$[k_L a]_d = [k_L a]_g - [k_L a]_f \quad (10)$$

C_o is the Cr(VI) concentration in the feed container (mg L^{-1}), C_s is the Cr(VI) concentration in the permeate container (mg L^{-1}), $[k_L a]_g$ is the global mass transfer factor (h^{-1}), β is the Cr(VI)-GMSPES membrane affinity parameter (g h mg^{-1}), q is the cumulative amount of Cr(VI) adsorbed into the GMSPES membrane (mg g^{-1}) and t is the time of the experiment (h), B is the potential mass transfer index related to the driving force of EMT (mg g^{-1}), $[k_L a]_f$ is the external mass transfer factor (h^{-1}), and $[k_L a]_d$ is the internal mass transfer factor (h^{-1}).

The verification of the parameters β and B was done by plotting $\ln(q)$ *versus* $\ln(t)$ according to eqn (7) to yield the linear function graph. Further, the computations of $[k_L a]_g$ accorded to C_o/C_s ratio and $[k_L a]_f$ accorded to q were made using eqn (8) and (9), respectively, while $[k_L a]_d$ was computed using eqn (10). An analysis of the variations of $[k_L a]_f$, $[k_L a]_d$ or $[k_L a]_g$ throughout the time t of the experiment permitted the prediction of the mechanisms and kinetics of mass transfer for the adsorption of Cr(VI) into the GMSPES membrane, which enabled the determination of MTR controlled by either EMT or IMT. The main concern of this study was the application of the GF equations in predicting the mass transfer phenomena, which is still rare and there have been limited studies on the EMT, IMT and GMT rates.

3. Results and discussion

3.1. Oxide composition and BET surface area of the GMS adsorbent

The GMS adsorbent (see Table 3) exhibited the oxide compositions of CaO (95.50%), Na_2O (1.62%), SrO (0.30%), Al_2O_3 (0.10%), Fe_2O_3 (0.02%) and K_2O (0.02%) from the EDXRF analysis. The compositions of major oxides, CaO and Na_2O, and minor oxides, SrO, Al_2O_3, Fe_2O_3 and K_2O, were verified for the GMS material. The determination of the specific surface area of the GMS adsorbent by the multiple-point method using the Surfer Analyzer of Thermo Scientific Flash 2000 Elemental Analyzer exhibited a BET surface area of 258.4 m^2 g^{-1}.[23]

3.2. Characteristics of the GMSPES membrane

3.2.1. Analysis of the SEM micrographs. An analysis of the SEM micrographs enabled the verification of the top surface and cross-sectional features of the GMSPES membranes with the magnifications of 1000 and 1500 times, respectively, for different GMS/PES ratios of 0.0, 0.5, 1.0 and 1.5 (see Fig. 2). The presence of GMS, which did not appear on the surface of GMSPES0.0 (see Fig. 2a-i), was clearly observed on the GMSPES0.5 (see Fig. 2b-i), GMSPES1.0 (see Fig. 2c-i) and GMSPES1.5 (see Fig. 2d-i) surfaces, as marked by the yellow circles. This indicated the impregnation of GMS into the PES matrix. SEM micrographs of the cross-sectional structures of GMSPES membranes exhibited the neat matrices of GMSPES0.0 (see Fig. 2a-ii) and GMSPES0.5 (see Fig. 2b-ii). The finger-like pore structure at the middle and narrow macrovoids at the bottom layer was observed for GMSPES0.0 (see Fig. 2a-ii). The elongated finger-like pore structure at the middle and broad macrovoids at the bottom layer was observed for GMSPES0.5 (see Fig. 2b-ii). The SEM micrograph of GMSPES0.5 scanned

Table 3 The EDXRF analysis of oxide compositions of the GMS adsorbent

Chemical composition oxides of GMS material (wt%)						
CaO	Na_2O	SrO	Al_2O_3	Fe_2O_3	K_2O	P_2O_5
95.50	1.62	0.30	0.10	0.02	0.02	ND

Note that ND means no detected oxide.

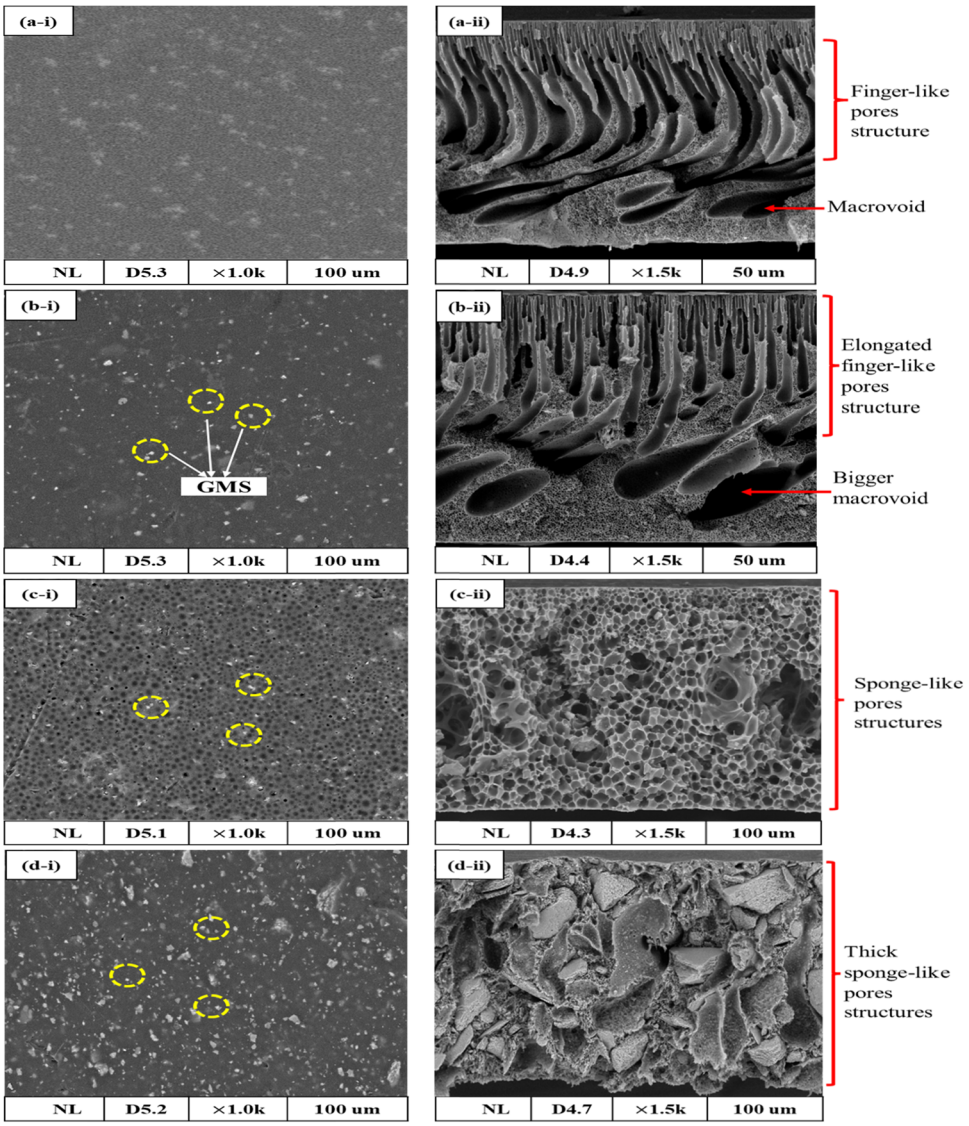

Fig. 2 SEM micrographs of the top surface remarked with (-i) and cross-section marked with (-ii) of the GMSPES membranes with (a) GMSPES0.0, (b) GMSPES0.5, (c) GMSPES1.0 and (d) GMSPES1.5.

with 1500 times magnification exhibited a rough surface with an increased size of the macrovoids and the different shapes of finger-like pores elongated toward the bottom part of the mixed matrix membrane with a GMS/PES ratio of 0.5 (see Fig. 2b-ii). This indicated the role of GMS in increasing the rate of phase inversion, leading to an increased velocity of water diffused into the casting solution.[35,36] The fairly fast diffusion of water induced during the phase inversion process by incorporating a small quantity of the hydrophilic GMS material resulted in the formation of a finger-like pore structure of the GMSPES0.5 membrane.[17] The formation of the sponge-like pore structure for the GMSPES1.5 membrane (see Fig. 2d-ii) was thicker compared to the GMSPES1.0 membrane (see Fig. 2c-ii) due to the ratio of GMS/PES increased by 50% from 1.0 to 1.5 (see Table 1), which raised the dope solution viscosity and a change in the structure of GMSPES membrane to slow down the penetration of water into a mixed matrix membrane. The inflow of water (nonsolvent) during the phase inversion process was hindered by incorporating a high quantity of the GMS material, resulting in less water being captured by the casting film, leading to a slow precipitation mode, resulting in the formation of a sponge-like pore structure of the GMSPES1.0 and GMSPES1.5 membranes.[37]

3.2.2. Analysis of the AFM images. The AFM images enabled the examination of the surface roughness of the GMSPES membranes and showed that the value of R_a increased from 1.24 μm for GMSPES0.0 to 6.96 μm for GMSPES0.5 to 18.81 μm for GMSPES1.0 and to 22.01 μm for GMSPES1.5 (see Fig. 3), with the amount of GMS incorporated with PES increasing from 0 to 10 to 20 and 30 g, respectively (see Table 1). It has been reported that the R_a values of 25.2 μm and 28.5 μm for the GMSPES membranes containing 40 g and 44 g of GMS, respectively, exhibited the impact of increasing the amount of GMS on the surface roughness of GMSPES membranes.[23] It was in

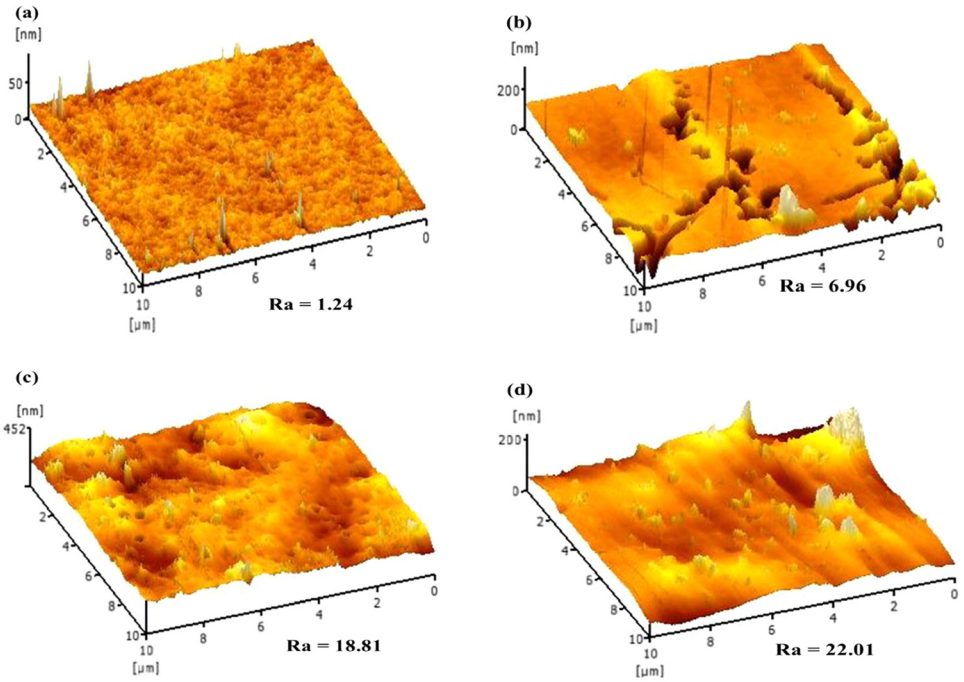

Fig. 3 AFM surface images for analyzing the surface roughness of the GMSPES membranes with (a) GMSPES0.0, (b) GMSPES0.5, (c) GMSPES1.0 and (d) GMSPES1.5.

agreement with a previous study showing that the value of R_a for the modified-clay/polyethersulfone mixed matrix membrane increased from 0.284 to 0.312 μm with an increased amount of modified-clay from 3 to 7 wt%.[38] A deviation of the membrane surface topography for GMSPES0.5, GMSPES1.0 and GMSPES1.5 from an ideal smooth surface of GMSPES0.0 was due to the incorporation of GMS into the GMSPES membrane during the phase inversion process.[39,40]

3.2.3. Analysis of WCA, PWF and porosity. The hydrophilicity of GMSPES characterized by WCA was due to the effect of GMS on the surface wettability. A decrease in the hydrophilicity of the GMSPES membrane leads to an increased WCA, which depends on the amount of GMS incorporated into PES.[41] The incorporation of GMS into the GMSPES membrane increased from 0 to 10 to 20 and to 30 g, which resulted in an increased tangent line of WCA from 63.9° to 64.4° to 65.3° and to 66.2° (see Table 4), which reduced the wettability of the GMSPES surface. The products of GMSPES0.0 without adding GMS and GMSPES0.5 incorporated with 10 g of GMS resulted in a finger-like pore structure of cross-section (see Fig. 2a-ii and b-ii) with a WCAs of 63.9° and 64.4°, respectively (see Table 4). The porous structure of GMSPES0.0 and GMSPES0.5, characterized by a low degree of WCA, had the potential to easily diffuse the water molecules, which was indicated by a high wettability.[42] The incorporation of 20 g and 30 g of GMS into the GMSPES membrane resulted in the WCA degrees of 65.3° for GMSPES1.0 and 66.2° for GMSPES1.5, respectively (see Table 4). This created the dense structure of the GMSPES membrane with tightly packed GMS particles, resulting in a sponge-like pore structure (see Fig. 2c-ii and d-ii), which hindered the diffusion of water molecules, indicating a low wettability.[43] On the contrary, when the incorporation of GMS increased from 0 g for the pure PES membrane to 40 and 44 g for the GMSPES membranes with the GMS/PES ratios of 2.0 and 2.2, respectively, the WCA degree decreased from 63.9° for GMSPES0.0 to 62.3° for GMSPES2.0 and to 60.5° for GMSPES2.2 because the formation of a rough surface increased with the increasing fraction of GMS incorporated into the GMSPES membrane.[23] The incorporation of salicylate-alumoxane nanoparticles (SAN) into the SAN mixed matrix polysulfone membrane decreased the degree of WCA and the wettability compared with neat polysulfone membrane.[44]

Table 4 Analysis of WCA, porosity and PWF for the GMSPES membranes

Membrane	GMS/PES ratio	WCA (°)	PWF (L m^{-2} h^{-1})	Porosity (%)
GMSPES0.0	0.0	63.9	15.25	43.13
GMSPES0.5	0.5	64.4	13.36	37.91
GMSPES1.0	1.0	65.3	11.72	36.62
GMSPES1.5	1.5	66.2	10.34	29.83

Note that WCA means water contact angle and PWF means pure water flux

The value of PWF decreased from 15.25 L m^{-2} h for GMSPES0.0 to 13.36 L m^{-2} h^{-1} for GMSPES0.5 to 11.72 L m^{-2} h^{-1} for GMSPES1.0 and to 10.34 L m^{-2} h^{-1} for GMSPES1.5 (see Table 4), which was due to the incorporation of GMS into the GMSPES membrane increasing from 0 to 10 to 20 and to 30 g (see Table 1). An increase in the amount of GMS incorporated with PES resulted in the formation of a compact, thick and dense GMSPES matrix,[45,46] which decreased the PWF

and porosity of the GMSPES membrane (see Table 4). The porosity of the GMSPES membrane decreased from 43.13% for GMSPES0.0 to 37.91% for GMSPES0.5 to 36.62% for GMSPES1.0 and to 29.83% for GMSPES1.5 (see Table 4). This exhibited that the increased incorporation of GMS from 0 to 10 to 20 and to 30 g increased the compact and bulk density of the mixed matrix membrane, decreasing the voids and porosity.[47,48]

3.3. Analysis of the FSAMCFTP performance

The FSAMCFTP performance was analyzed to determine the efficiency and adsorption capacity of the FSAMCFTP process by monitoring the Cr(VI) concentrations before and after passing through the GMSPES membrane. There is no data on the efficiency of Cr(VI) removal for GMSPES0.0, *i.e.*, without the GMS adsorbent. The plot of *E versus t* exhibited a trend of decreasing *E* and that of plotting *q versus t* exhibited a trend of increasing *q* with increasing *t* throughout the 3.5 h experiment (see Fig. 4). The performances of the FSAMCFTP process at 0.08 h of the experiment increased from 26.63% for GMSPES0.5 with its total surface area (TSA) of 2584 m^2 to 43.78% for GMSPES1.0 with its TSA of 5168 m^2 and to 60.69% of efficiency for the GMSPES1.5 with its TSA of 7752 m^2 (see Fig. 4a–c, dashed line), which were due to the increasing amount of GMS from 10 g to 20 g and to 30 g (see Table 1). The surface area and number of active sites increased with an increased amount of GMS incorporated with PES, which had the potential to increase the adsorption affinity of the GMSPES membrane to attract Cr(VI) ions from SS.[13] An increase in the amount of GMS incorporated into the GMSPES membrane increased the surface area and number of active sites due to the increased attractive forces between the GMS and Cr(VI) ions.[42] The Cr(VI) removal efficiencies of 16.05% for GMSPES incorporated with 40 g and 10.75% for GMSPES incorporated with 44 g of GMS at 0.08 h of the experiment exhibited that by increasing the amount of GMS higher than 40 g led to a decreased efficiency.[23] The removal efficiencies of Cr(VI) decreased by 26.51% from 26.63% to 0.12% for GMSPES0.5, by 43.70% from 43.78% to 0.08% for GMSPES1.0 and by 60.59% from 60.69% to 0.10% for GMSPES1.5 were verified from 0.08 h to 3.5 h of the experiment (see Fig. 4a–c; dashed line). This suggested the attraction of Cr(VI) affected by continuously occupying the active sites of CaO and Al_2O_3 on the surface of GMSPES membrane resulted in the formation[49] of the solid solutions such as $3CaO{\cdot}Al_2O_3{\cdot}CaCrO_4{\cdot}nH_2O$ leading to decrease the performance of FSAMCFTP process. The best performance of the GMSPES membrane to remove Cr(VI) from SS ranged from 24.50 to 26.63% for GMSPES0.5, from 34.75 to 43.78% for GMSPES1.0 and from 39.26 to 60.69% for the GMSPES1.5 membrane (see Fig. 4a–c; dashed line) during 1.0 h at the beginning were higher compared to that ranging from 15.00 to 16.05% for GMSPES2.0 and from 10.00 to 10.75% for the GMSPES2.2 membrane at the start of the experiment for 1.5 h.[23] This showed that the removal efficiency of Cr(VI) was decreased by adding 40 g or higher amounts of GMS incorporated into 20 g of PES to create the GMSPES membrane. The decreasing trend of *E* throughout the time *t* of the experiment was related to the active sites of CaO occupied by the Cr(VI) ions, which was dependent on the amount of GMS incorporated into the GMSPES membrane (see Fig. 4a–c; dashed line). A decreased efficiency of Cr(VI) removal was related to an increased occupation of the interstitial surface area of the voids and pores per unit mass of the GMS and acceptor sites of different oxides by the adsorption of Cr(VI) ions, leading to continuously decreased interaction between the GMS and Cr(VI) during the experiment.[23]

The adsorption capacity of GMSPES increased throughout the 3.5 h of the experiment and was related to the electrostatic force of attraction (see Fig. 4a–c; solid line). This indicated that the occupation of the GMS by Cr(VI) ions continuously increased due to the availability of active sites that still existed during the adsorption process. The adsorption capacities of 13.4 mg g^{-1} for GMSPES0.5, 15.2 mg g^{-1} for GMSPES1.0 and 10.8 mg g^{-1} for GMSPES1.5 exhibited an entry of Cr(VI) into the GMSPES membrane (see Fig. 4a–c; solid line). This was supported by an analysis of the EDX spectra showing the Cr(VI)

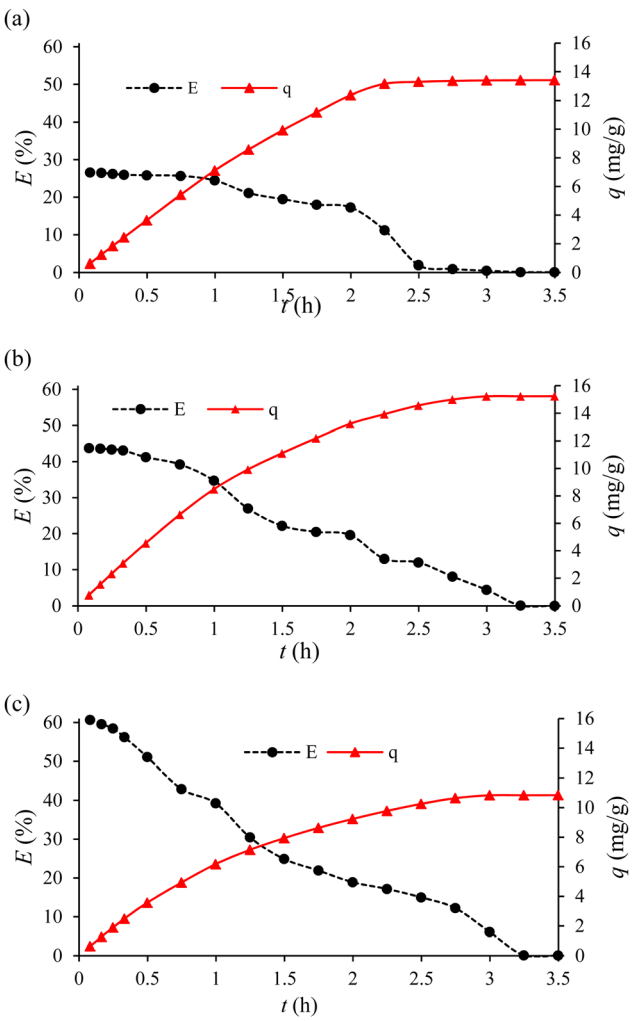

Fig. 4 Performance analysis of *E versus t* and *q versus t* for the adsorption of Cr(VI) from SS into the GMSPES membranes with (a) GMSPES0.5, (b) the GMSPES1.0 and (c) GMSPES1.5.

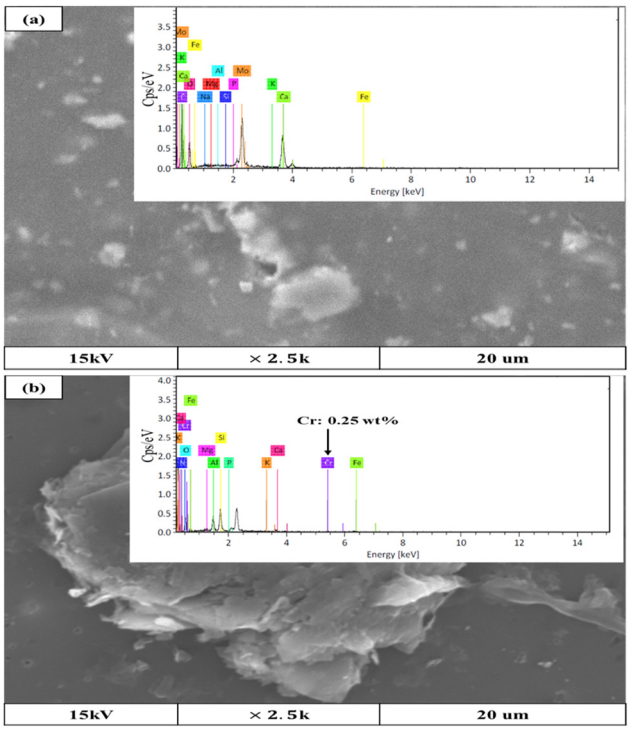

Fig. 5 The EDX spectra analysis of the GMSPES membrane (a) before the adsorption of Cr(VI) and (b) after the adsorption of Cr(VI).

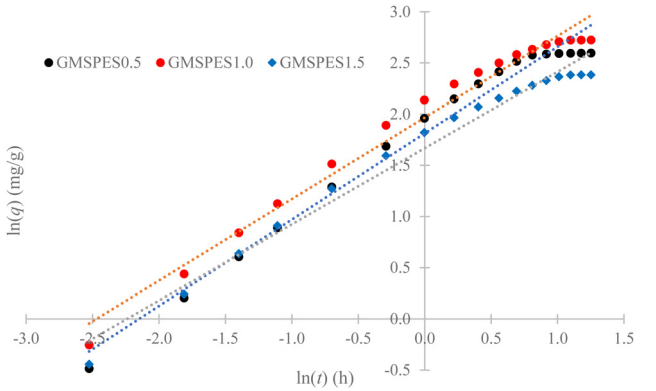

Fig. 6 Linear regression analysis by plotting ln(q) *versus* ln(t) to gain the correlation between the parameters β and B for calculating the variations of $[k_La]_g$, $[k_La]_f$ and $[k_La]_d$ throughout the 3.5 h experiment.

Table 5 Verification of the parameters β and B for calculating $[k_La]_f$, $[k_La]_d$ and $[k_La]_g$

Adsorptive membrane	β (g h mg^{-1})	B (mg g^{-1})	R^2
GMSPES0.5	1.1855	1.8131	0.9802
GMSPES1.0	1.2555	1.9670	0.9797
GMSPES1.5	1.3432	1.6677	0.9793

element captured by the GMSPES membrane after the adsorption process (see Fig. 5b), which did not appear before the adsorption of Cr(VI) ions (see Fig. 5a). The maximum adsorption capacity of 89.16 mg g^{-1} was obtained for the removal of Cr(VI) from wastewater by the composite adsorptive membrane modified with polyethyleneimine along with fast adsorption kinetics after 100 min of the experiment.[50] The investigation of the GMSPES membrane for removing Cr(VI) from SS offers an effort to establish the principles and procedures that can be extended for the treatment of real wastewater, which contains organic and inorganic pollutants. The application of the GMSPES membrane can be extended to remove Cr(VI) from industrial wastewater by first subjecting it to preliminary treatments, such as the hybrid separation process consisting of a fixed-bed column to remove impurities.[28,31] The incorporation of GMS with PES to synthesize an adsorptive membrane is a promising method for removing Cr(VI) from aqueous solutions.

3.4. Analysis of the mass transfer kinetics

3.4.1. Analysis of the linear function. The plot of ln(q) on the y-axis *versus* ln(t) on the x-axis, according to eqn (7), resulted in a linear graph with a slope of $1/\beta$ and the y-intercept of B (see Fig. 6). All graphs of linear function had excellent correlation between the parameters of β and B with $R^2 > 0.9793$ (see Table 5). The variations of $[k_La]_f$, $[k_La]_d$ and $[k_La]_g$ according to t were calculated using eqn (9), eqn (10) and eqn (8), respectively. The adsorption of Cr(VI) into the GMSPES membrane could theoretically include three stages: EMT, IMT and fixation. However, the fixation of Cr(VI) onto the surface of GMS was very fast and negligible in determining the MTR during the adsorption process.[29] The incorporation of GMS with PES had an impact on adsorbing Cr(VI) from SS into the GMSPES membrane and also on the mechanisms and kinetics of EMT, IMT and GMT, which was controlled by the driving force of EMT from bulk SS to the film zone and then by the diffusion force of IMT within the pores of GMS. The value of β increased from 1.1855 to 1.2555 and to 1.3432 g h mg^{-1} (see Table 5) in accordance with the amount of GMS increasing from 10 to 20 and to 30 g (see Table 1), contributing to an increased number of active sites like CaO and Na_2O and the availability of surface area per unit mass of the GMS adsorbent, affecting the mass transfer kinetics of Cr(VI) removed from SS.[51] The B values of 1.8131, 1.9670 and 1.6677 mg g^{-1} in ln(q) were related to 6.13, 7.15 and 5.30 g of Cr(VI) adsorbed into GMSPES0.5, GMSPES1.0 and GMSPES1.5, respectively, during 1.0 h of the experiment (see Table 5), and contributed to the adsorption capacities of 13.41, 15.24 and 10.84 mg g^{-1}, respectively, for the 3.5 h experiment (see Fig. 4). The electrostatic force of Cr(VI) attracted by the active sites of CaO and Na_2O was dependent on the rate-limiting steps of EMT and IMT. To have a comprehensive understanding of Cr(VI) adsorbed into the GMSPES membrane by the FSAMCFTP process, the behavioral mechanisms and kinetics of EMT, IMT and GMT were predicted using the GF equations. For this study, using the GMSPES membrane with different GMS/PES ratios of 0.0, 0.5, 1.0 and 1.5 enabled the prediction of the variations of $[k_La]_f$, $[k_La]_d$ and $[k_La]_g$, which represented the rates of EMT, IMT and GMT, respectively, throughout the 3.5 h experiment. MTR was determined by comparing the rate of EMT to IMT at each

comparative point. The findings of this study, supported by the previous FSAMCFTP experiment using the GMS/PES ratios of 0.0, 2.0 and 2.2, provide a fairly comprehensive understanding of the mass transfer kinetic behaviors of Cr(VI) adsorbed into the GMSPES membrane. The originality of this work is expanding the application of GF equations for the prediction of the behavioral mass transfer kinetics of Cr(VI) adsorbed into the GMSPES membrane using the low GMS/PES ratios of 0.0, 0.5, 1.0 and 1.5, which is expected to contribute to the advancement of adsorptive membrane technology.

3.4.2. Analysis of the kinetics of EMT, IMT and GMT. Using the GF equations permitted the prediction of the mechanisms and mass transfer kinetics of Cr(VI) removed from SS by the FSAMCFTP process, which enabled the analysis of the EMT, IMT and GMT rates. The variations of $[k_La]_f$, $[k_La]_d$ and $[k_La]_g$ throughout the 3.5 h experiment were subject to the rates of EMT, IMT and GMT, respectively (see Fig. 7). The variations of $[k_La]_f$, $[k_La]_d$ and $[k_La]_g$ exhibited an almost similar trend and increased the amount of GMS incorporated into the GMSPES membrane and the time of the experiment on the rates of EMT, IMT and GMT. A decrease in the rate of EMT counterbalanced by an increased rate of IMT resulted in the rate of GMT as the sum of EMT and IMT decreased throughout the 3.5 h experiment. The rate of EMT rapidly decreased at the beginning for 0.5 h and then continued to slowly decrease for 3.0 h from 0.5 to 3.5 h of the experiment, which was dependent on the availability of active sites occupied by the Cr(VI) ions, which led to a decreased driving force of transporting Cr(VI) from bulk SS to the film zone near the surface of the GMS adsorbent. The variation of $[k_La]_f$ ranged from 0.5567 to 4.7259 h^{-1} for GMSPES0.5, which was lower than that ranging from 0.9388 to 9.3540 h^{-1} for GMSPES1.0 and from 1.2188 to 15.9045 h^{-1} for GMSPES1.5 during the initial 0.5 of the experiment (see Fig. 7a–c; black color). This indicated an increased amount of GMS incorporated into the GMSPES membrane, which increased the number of active sites and surface area of the GMS adsorbent and impacted the rate of EMT. The rapid movement of Cr(VI) from the bulk water to the film zone at the beginning of the experiment was due to the availability of acceptor sites in a large-area open surface, which impacted the driving force controlling the EMT rate on the attraction of Cr(VI) with the GMS adsorbent.[52,53] The rate-limiting step of mass transfer for the adsorption of Cr(VI) into the GMSPES membrane by the FSAMCFTP process was progressively controlled by the rate of EMT, which was dependent on the driving force of transporting the Cr(VI) ions from the bulk SS to film zone near the GMS adsorbent surface.

The adsorption kinetic limitation of Cr(VI) diffused in the GMS matrix is controlled by the IMT rate, which exhibited all negative values of $[k_La]_d$ at 0.08 h of the experiment (see Fig. 7a–c; red color). Therefore, the $[k_La]_d$ value of −2.0686 h^{-1} for GMSPES0.5 was higher than that of −2.5496 h^{-1} for GMSPES1.0, which was higher than that of −7.1344 h^{-1} for GMSPES1.5, which depended on the wettability and density of the GMSPES membrane. This indicated the increased hydrophilicity of the GMSPES membrane by decreasing the amount

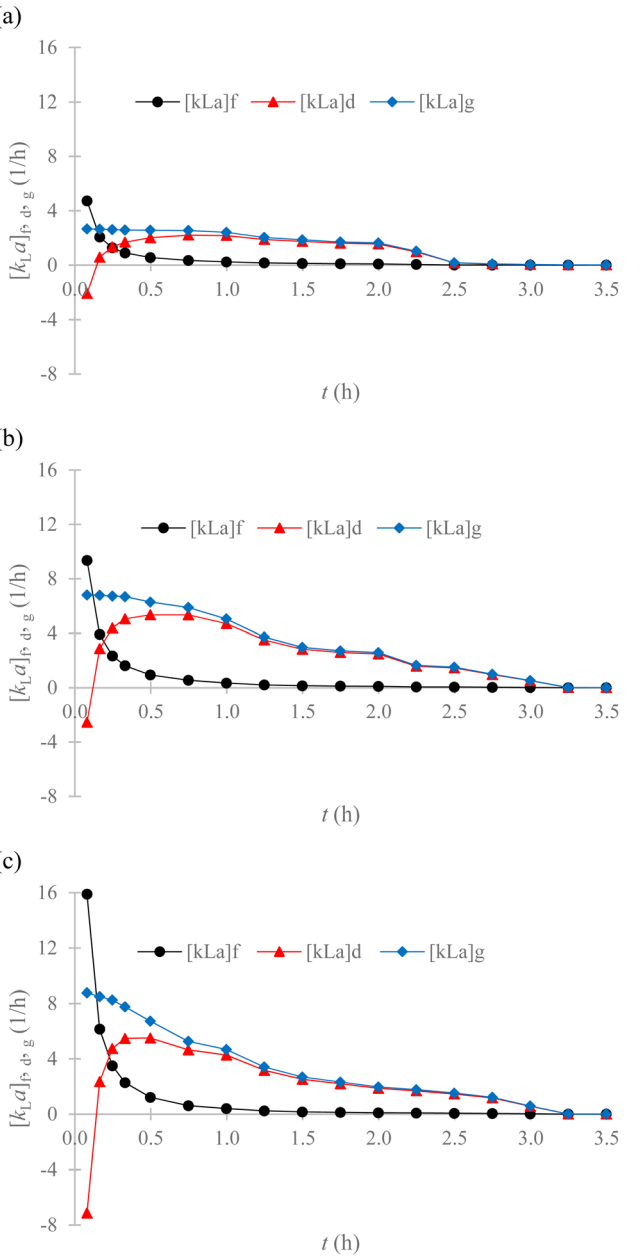

Fig. 7 Analysis of the EMT, IMT and GMT rates for the adsorption of Cr(VI) from SS on the GMSPES membranes using (a) GMSPES0.5, (b) the GMSPES1.0 and (c) GMSPES1.5.

of GMS, causing an increased rate of IMT, which enhanced the performance of the FSAMCFTP process. An analysis of the performances of FSAMCFTP influenced by the EMT, IMT and GMT rates was made by scrutinizing the variations of $[k_La]_f$, $[k_La]_d$ and $[k_La]_g$, respectively, according to t of the experiment. The variations of $[k_La]_d$ increased by 197.15% from −2.0686 to 2.0096 h^{-1} for GMSPES0.5, by 309.770% from −2.5496 to 5.3465 h^{-1} for GMSPES1.0 and by 177.22% from −7.1344 to 5.5095 h^{-1} for GMSPES1.5, which were verified from 0.08 to 0.5 h of the experiment. This indicated that an increased amount of GMS from 10 to 20 and to 30 g into the GMSPES membrane impacted the diffusion behavior of Cr(VI) through

the pores. The diffusion of Cr(VI) through the GMS matrix increased from 0.08 to 0.5 h and then gradually decreased from 0.5 to 2.5 h for GMSPES0.5 and from 0.5 to 3.25 h for GMSPES1.0 and GMSPES1.5 and then slowly decreased until 3.5 h of the experiment. The accessibility of the pore structure for different GMS/PES ratios of the GMSPES membrane was different in the diffusion of Cr(VI) ions with the pores in spite of the GMS adsorbent having the same BET surface area of 258.4 m^2/g.[54] The variations of $[k_La]_d$ rapidly increased from −2.0686 to 2.0096 h^{-1}, from −2.5496 to 5.3465 h^{-1} and from −7.1344 to 5.5095 h^{-1} (see Fig. 7a–c; red color), which were counterbalanced by a decrease in the variations of $[k_La]_f$ from 4.7259 to 0.5567 h^{-1}, from 9.3540 to 0.9388 h^{-1} and from 15.9045 to 1.2188 h^{-1} (see Fig. 7a–c; black color), respectively, resulting in the $[k_La]_g$ slowly decreasing from 2.6573 to 2.5663 h^{-1}, from 6.8044 to 6.2853 h^{-1} and from 8.8801 to 6.7283 h^{-1} (see Fig. 7a–c; blue color) observed for the adsorptive membranes of GMSPES0.5, GMSPES1.0 and GMSPES1.5, respectively, from 0.08 to 0.5 h of the experiment. This suggested that the rate-limiting step of Cr(VI) adsorption was firstly controlled by the IMT rate for 0.17 h from 0.08 to 0.25 h and then dominantly controlled by the rate of EMT after 0.25 h of the experiment.

The FSAMCFTP process to remove Cr(VI) from SS was performed with the low GMS/PES ratios of 0.0, 0.5, 1.0 and 1.5. The GF equations could be useful in investigating the EMT, IMT and GMT rates for the adsorption of Cr(VI) from SS. An analysis of the EMT and IMT rates enabled the prediction of MTR to gain an understanding of the rate-limiting step of Cr(VI) removed by the FSAMCFTP process. An in-depth understanding of response mechanisms of the GMSPES membrane is necessary to elucidate the interfacial flow patterns and dynamic response diffusion mechanisms of Cr(VI) adsorption.[55] A decrease in the rate of EMT counterbalanced with an increased rate of IMT led to a decrease in the GMT rate for 0.42 h from 0.08 to 0.5 h of the experiment. It was due to an increased occupation of the GMS surface, which decreased the driving force of EMT and increased the diffusion force of Cr(VI) moving within the pores on the adsorption kinetics of GMT. The precipitation of concentrated Cr(VI) after passing through a film zone at the GMS surface had the driving force decreased, as shown by the $[k_La]_f$, which is decreased by 88.22% from 4.7259 to 0.5567 h^{-1} for GMSPES0.5, by 89.96% from 9.3540 to 0.9388 h^{-1} for GMSPES1.0 and by 92.34% from 15.9045 to 1.2188 h^{-1} for GMSPES1.5 from 0.08 to 0.5 h of the experiment (see Fig. 7a–c; black color). The rate of driving force reduction was dependent on the distribution of active sites and the surface area of the GMS incorporated into the GMSPES membrane.[56] The findings of this study provided insight into the GMT rate controlled by the IMT rate for 0.08 h and then dominated by the EMT rate for 3.0 h of the experiment. This study contributes to enriching our understanding of Cr(VI) adsorption by the GMSPES membrane applied in the FSAMCFTP process and advancing the applications of adsorptive membrane technology in the treatment of Cr(VI)-contaminated water.

3.5. Correlation between E and $[k_La]_d$

The scientific concern of this study was to build a support knowledge base in designing the FSAMCFTP process with chemical-less and environmentally friendly separation methods from the analysis of GMT rates. This enabled the development of rapid and effective adsorption of Cr(VI) from SS.[57] The dependence of Cr(VI) removal efficiency on the GMT rate was analyzed by plotting the graph of E *versus* $[k_La]_g$, as shown in Fig. 8, which was based on the fact that the rate of GMT regularly decreased throughout the 3.5 h experiment (see Fig. 7a–c; blue color). This exhibited that the adsorption of Cr(VI) evenly decreased over time and still continued throughout the 3.5 h experiment. The rate of EMT rapidly decreased at the beginning for 0.08 h from 0.08 to 0.16 h and then slowly for 3.0 h from 0.25 to 3.25 h of the experiment, which resulted in the rate of GMS as the sum of EMT and IMT regularly decreasing throughout the 3.5 h experiment. The efficiency of Cr(VI) removal for all GMSPES membranes linearly increased with increasing GMT rate (see Fig. 8). The maximum Cr(VI) removal efficiencies of 26.63, 43.78 and 60.69% obtained at the $[k_La]_g$ values of 2.6573, 6.8044 and 8.7701 h^{-1} for GMSPES0.5, GMSPES1.0 and GMSPES1.5, respectively, had a significant impact of increasing the number of active sites and surface area of GMS and subsequently on the adsorption capacity. The rate of GMT decreased throughout the 3.5 h adsorption process was dependent on the mass transfer kinetics of Cr(VI) removal, which can be optimized by simultaneously increasing the number of active sites and surface area of GMS before incorporating into the GMSPES membrane.

The removal efficiencies of Cr(VI) ranged from 11.23 to 26.63% with $[k_La]_g$ ranging from 1.0216 to 2.6573 h^{-1} for GMSPES0.5 during 2.25 h, from 12.00 to 43.78% with $[k_La]_g$ ranging from 1.1506 to 6.8044 h^{-1} for GMSPES1.0 during 2.5 h and from 12.24 to 60.69% with $[k_La]_g$ ranging from 1.2265 to 8.7701 h^{-1} for GMSPES1.5 during 2.75 h of the experiment. This was due to an increased number of CaO, Na_2O, SrO and Al_2O_3 by increasing the amount of GMS incorporated with PES, which resulted in an increased performance of the FSAMCFTP process.[58] The plot (Fig. 8) of E *versus* $[k_La]_g$ provided a linear equation in the form: $E = [k_La]_g + b$ with $R^2 > 0.9862$ (see Table 6),

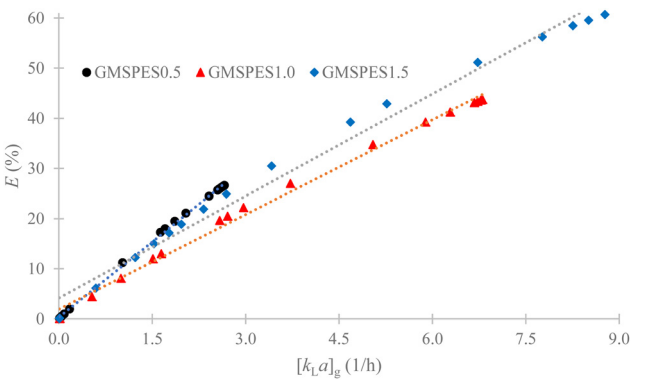

Fig. 8 Analysis of the correlation between E and $[k_La]_g$ for evaluating the effect of the GMT rate on the efficiency of Cr(VI) removal.

Table 6 Values of a as the t slope and b as the y-intercept, obtained by plotting E *versus* $[k_La]_g$

Adsorptive membrane	a (g h mg^{-1})	b (mg g^{-1})	R^2
GMSPES0.5	10.1038	0.3147	0.9988
GMSPES1.0	6.3004	1.9184	0.9946
GMSPES1.5	6.7946	4.1258	0.9862

where a is the slope and b is the y-intercept. Using this linear equation enabled the prediction of an upper ceiling of 100% efficiency by conditioning an increased rate of GMT in the FSAMCFTP process at the $[k_La]_g$ values of 9.8661 h^{-1} for GMSPES0.5, 15.5675 h^{-1} for GMSPES1.0 and 14.1106 h^{-1} for GMSPES1.5. Efforts to increase the rate of GMT related to the number of active sites and porosity of the GMS adsorbent can be suggested by the physical and chemical activation methods to increase the distribution of active sites and to expand the surface area of GMS before incorporating with PES to synthesize the GMSPES membrane.

4. Conclusions

Applying the GF equations permitted the prediction of the adsorption kinetics of Cr(VI) by the GMSPES membrane in the FSAMCFTP process. Removal efficiencies of 26.63, 43.78 and 60.69% and adsorption capacities of 13.4, 15.2, and 10.8 mg g^{-1} were obtained for the adsorption of Cr(VI) by the GMSPES0.5, GMSPES1.0 and GMSPES1.5 membranes, respectively. The behavioral adsorption kinetics of Cr(VI) subjected to the EMT, IMT and GMT rates were different, even though a similar trend in the variations of $[k_La]_f$, $[k_La]_d$ and $[k_La]_g$ was verified due to the different amounts of GMS incorporated into the GMSPES membrane. By comparing the EMT with the IMT rates of Cr(VI) transport from SS toward the acceptor sites of GMS, the prediction of MTR was enabled, which was dependent on the IMT rate at the beginning for 0.08 h and then dominantly controlled by the EMT rate for 3.0 h of the experiment. An analysis of the correlation between E and $[k_La]_g$ provides insight into the advancement of the FSAMCFTP process, enriching the field of adsorptive membrane technology and optimizing the Cr(VI) removal efficiency.

Data availability

The data that support the findings of this study are available from the corresponding author, M. A. F., upon reasonable request.

Conflicts of interest

The authors declare no competing interests associated with this manuscript.

Acknowledgements

The authors thank financial support from the Ministry of Higher Education – Malaysia for the Higher Institution Centre of Excellent (HICoE) Grant Scheme No. R.J090301.7851.4J517. All the funding bodies have no role in the design of the study, collection, analysis and interpretation of data, and writing this manuscript. The authors gratefully acknowledge the Advance Membrane Technology Research Centre (AMTEC) and the Environmental Laboratory of the Faculty of Civil Engineering, Universiti Teknologi Malaysia, for the laboratory facilities and technical staff for their technical assistance during the experiment.

References

1 K. E. Ukhurebor, U. O. Aigbe, R. B. Onyancha, W. Nwankwo, O. A. Osibote and H. K. Paumo, *et al.*, Effect of hexavalent chromium on the environment and removal techniques: A review, *J. Environ. Manage.*, 2021, **280**, 111809, DOI: 10.1016/j.jenvman.2020.111809.

2 S. S. Kerur, S. Bandekar, M. S. Hanagadakar, S. S. Nandi, G. M. Ratnamala and P. G. Hegde, Removal of hexavalent Chromium-Industry treated water and wastewater: A review, *Mater. Today: Proc.*, 2020, **42**, 1112–1121, DOI: 10.1016/j.matpr.2020.12.492.

3 P. Sharma, S. P. Singh, S. K. Parakh and Y. W. Tong, Health hazards of hexavalent chromium (Cr(VI)) and its microbial reduction, *Bioengineered*, 2022, **13**, 4923–4938, DOI: 10.1080/21655979.2022.2037273.

4 D. Chen, X. Xiao and K. Yang, Removal of phosphate and hexavalent chromium from aqueous solutions by engineered waste eggshell, *RSC Adv.*, 2016, **6**, 35332–35339, DOI: 10.1039/c6ra05034d.

5 R. O. Oruko, J. N. Edokpayi, T. A. M. Msagati, N. T. Tavengwa, H. J. O. Ogola and G. Ijoma, *et al.*, Investigating the chromium status, heavy metal contamination, and ecological risk assessment via tannery waste disposal in sub-Saharan Africa (Kenya and South Africa), *Environ. Sci. Pollut. Res.*, 2021, **28**, 42135–42149, DOI: 10.1007/s11356-021-13703-1.

6 M. Tumolo, V. Ancona, D. De Paola, D. Losacco, C. Campanale and C. Massarelli, *et al.*, Chromium pollution in European water, sources, health risk, and remediation strategies: An overview, *Int. J. Environ. Res. Public Health.*, 2020, **17**, 1–25, DOI: 10.3390/ijerph17155438.

7 A. Mishra, B. D. Tripathi and A. K. Rai, Packed-bed column biosorption of chromium(VI) and nickel(II) onto Fenton modified Hydrilla verticillata dried biomass, *Ecotoxicol. Environ. Saf.*, 2016, **132**, 420–428, DOI: 10.1016/j.ecoenv.2016.06.026.

8 N. Hayashi, D. Matsumura, H. Hoshina, Y. Ueki, T. Tsuji and J. Chen, *et al.*, Chromium(VI) adsorption–reduction using a fibrous amidoxime-grafted adsorbent, *Separ. Purif. Technol.*, 2021, **277**, 119536, DOI: 10.1016/j.seppur.2021.119536.

9 S. Aoudj, A. Khelifa, N. Drouiche, R. Belkada and D. Miroud, Simultaneous removal of chromium(VI) and fluoride by

electrocoagulation–electroflotation: Application of a hybrid Fe-Al anode, *Chem. Eng. J.*, 2015, **267**, 153–162, DOI: 10.1016/j.cej.2014.12.081.

10 A. Bratovcic, H. Buksek, C. Helix-Nielsen and I. Petrinic, Concentrating hexavalent chromium electroplating wastewater for recovery and reuse by forward osmosis using underground brine as draw solution, *Chem. Eng. J.*, 2022, **431**, 133918, DOI: 10.1016/j.cej.2021.133918.

11 M. F. Ahmed and M. B. Mokhtar, Assessing cadmium and chromium concentrations in drinking water to predict health risk in Malaysia, *Int. J. Environ. Res. Public Health*, 2020, **17**, 2966, DOI: 10.3390/ijerph17082966.

12 M. S. Samuel, E. Selvarajan, R. Chidambaram, H. Patel and K. Brindhadevi, Clean approach for chromium removal in aqueous environments and role of nanomaterials in bioremediation: Present research and future perspective, *Chemosphere*, 2021, **284**, 131368, DOI: 10.1016/j.chemosphere.2021.131368.

13 Y. J. Kim, J. Park, J. Bang, J. Kim, H.-J. Jin and H. W. Kwak, Highly efficient Cr(VI) remediation by cationic functionalized nanocellulose beads, *J. Hazard. Mater.*, 2022, **426**, 128078, DOI: 10.1016/j.jhazmat.2021.128078.

14 C. A. Papadimitriou, G. Krey, N. Stamatis and A. Kallianiotis, The use of waste mussel shells for the adsorption of dyes and heavy metals, *J. Chem. Technol. Biotechnol.*, 2017, **92**, 1943–1947, DOI: 10.1002/jctb.5247.

15 K. C. Khulbe and T. Matsuura, Removal of heavy metals and pollutants by membrane adsorption techniques, *Appl. Water Sci.*, 2018, **8**, 1–30, DOI: 10.1007/s13201-018-0661-6.

16 M. R. Adam, M. H. D. Othman, T. A. Kurniawan, M. H. Puteh, A. F. Ismail and W. Khongnakorn, *et al.*, Advances in adsorptive membrane technology for water treatment and resource recovery applications: A critical review, *J. Environ. Chem. Eng.*, 2022, **10**, 107633, DOI: 10.1016/j.jece.2022.107633.

17 M. Mondal, M. Dutta and S. De, A novel ultrafiltration grade nickel iron oxide doped hollow fiber mixed matrix membrane: Spinning, characterization and application in heavy metal removal, *Separ. Purif. Technol.*, 2017, **188**, 155–166, DOI: 10.1016/j.seppur.2017.07.013.

18 A. Kolbasov, S. Sinha-Ray, A. L. Yarin and B. L. Pourdeyhimi, Heavy metal adsorption on solution-blown biopolymer nanofiber membranes, *J. Membr. Sci.*, 2017, **530**, 250–263, DOI: 10.1016/j.memsci.2017.02.019.

19 L. Qalyoubi, A. Al-Othman and S. Al-Asheh, Recent progress and challenges on adsorptive membranes for the removal of pollutants from wastewater. Part I: Fundamentals and classification of membranes. Case Study, *Chem. Environ. Eng.*, 2021, **3**, 100086, DOI: 10.1016/j.cscee.2021.100086.

20 S. Bandehali, F. Parvizian, H. Ruan, A. Moghadassi, J. Shen and A. Figoli, *et al.*, A planned review on designing of high-performance nanocomposite nanofiltration membranes for pollutants removal from water, *J. Ind. Eng. Chem.*, 2021, **101**, 78–125, DOI: 10.1016/j.jiec.2021.06.022.

21 R. Ismail, D. F. Fitriyana, Y. I. Santosa, S. Nugroho, A. J. Hakim and M. S. Al Mulqi, *et al.*, The potential use of green mussel (*Perna Viridis*) shells for synthetic calcium carbonate polymorphs in biomaterials., *J. Crystal Growth.*, 2021, **572**, 126282, DOI: 10.1016/j.jcrysgro.2021.126282.

22 A. Mittal, M. Teotia, R. K. Soni and J. Mittal, Applications of egg shell and egg shell membrane as adsorbents: A review, *J. Mol. Liq.*, 2016, **223**, 376–387, DOI: 10.1016/j.molliq.2016.08.065.

23 M. A. Fulazzaky, N. A. A. Salim, M. H. Puteh, T. Messer, M. H. D. Othman and J. Jaafar, *et al.*, Mechanisms and mass transfer kinetics of Cr(VI) adsorbed by mussel shell incorporated adsorptive membrane, *Desalin. Water Treat.*, 2024, **319**, 100537, DOI: 10.1016/j.dwt.2024.100537.

24 I. Ali, O. A. Bamaga, L. Gzara, M. Bassyouni, M. H. Abdel-Aziz and M. F. Soliman, *et al.*, Assessment of blend PVDF membranes, and the effect of polymer concentration and blend composition, *Membranes*, 2018, **8**, 13, DOI: 10.3390/membranes8010013.

25 S. L. Duraikkannu, R. Castro-Muñoz and A. Figoli, A review on phase-inversion technique-based polymer microsphere fabrication, *Colloid Interface Sci. Commun.*, 2021, **40**, 100329, DOI: 10.1016/j.colcom.2020.100329.

26 M. Xiao, F. Yang, S. Im, D. S. Dlamini, D. Jassby and S. Mahendra, *et al.*, Characterizing surface porosity of porous membranes via contact angle measurements, *J. Membr. Sci. Lett.*, 2022, **2**, 100022, DOI: 10.1016/j.memlet.2022.100022.

27 E. W. Rice, R. B. Baird and A. D. Eaton, *Standard methods for the examination of water and wastewater*, 23rd edn, American Water Works Association, 2017.

28 M. A. Fulazzaky, M. H. Khamidun, M. F. M. Din and A. R. M. Yusoff, Adsorption of phosphate from domestic wastewater treatment plant effluent onto the laterites in a hydrodynamic column, *Chem. Eng. J.*, 2014, **258**, 10–17, DOI: 10.1016/j.cej.2014.07.092.

29 M. A. Fulazzaky, Determining the resistance of mass transfer for adsorption of the surfactants onto granular activated carbons from hydrodynamic column, *Chem. Eng. J.*, 2011, **166**, 832–840, DOI: 10.1016/j.cej.2010.11.052.

30 M. Wajdi, K. Muda and M. Fulazzaky, Mass transfer kinetics of chemical oxygen demand removed from palm oil mill effluent in stirred cylinder batch reactor, *J. Ind. Eng. Chem.*, 2023, **126**, 611–620, DOI: 10.1016/j.jiec.2023.06.053.

31 N. A. A. Salim, M. A. Fulazzaky, M. H. Puteh, M. H. Khamidun, A. R. M. Yusoff and N. H. Abdullah, *et al.*, Mass transfer kinetics and mechanisms of phosphate adsorbed on waste mussel shell, *Water, Air, Soil Pollut.*, 2022, **233**, 223, DOI: 10.1007/s11270-022-05693-8.

32 K. Muda, M. A. Fulazzaky, T. Messer, A. H. Omar and A. I. Omoregie, Mass transfer mechanisms and decolorization kinetics of the mixed azo dyes, *ACS ES&T Eng.*, 2024, **4**, 2381–2392, DOI: 10.1021/acsestengg.4c00258.

33 M. F. Fachrul, M. A. Fulazzaky, A. Rinanti, K. Muda, T. Tazkiaturrizki and T. Sunaryo, Mass transfer kinetics of polyethylene degradation by bacterial-fungal consortium, *Clean. Waste Syst.*, 2024, **7**, 100136, DOI: 10.1016/j.clwas.2024.100136.

34 M. A. Fulazzaky, M. H. Khamidun and R. Omar, Understanding of mass transfer resistance for the adsorption of solute onto porous material from the modified mass transfer factor models, *Chem. Eng. J.*, 2013, **228**, 1023–1029, DOI: 10.1016/j.cej.2013.05.100.

35 A. I. Nazri, A. L. Ahmad and M. H. Hussin, Microcrystalline cellulose-blended polyethersulfone membranes for enhanced water permeability and humic acid removal, *Membranes*, 2021, **11**, 660, DOI: 10.3390/membranes11090660.

36 F. Rafieian, M. Mousavi, A. Dufresne and Q. Yu, Polyethersulfone membrane embedded with amine functionalized microcrystalline cellulose, *Int. J. Biol. Macromol.*, 2020, **164**, 4444–4454, DOI: 10.1016/j.ijbiomac.2020.09.017.

37 X. Dong, A. Al-Jumaily and I. C. Escobar, Investigation of the use of a bio-derived solvent for non-solvent-induced phase separation (NIPS) fabrication of polysulfone membranes, *Membranes*, 2018, **8**, 23, DOI: 10.3390/membranes8020023.

38 M. Mahmoudian, P. G. Balkanloo and E. Nozad, A facile method for dye and heavy metal elimination by pH sensitive acid activated montmorillonite/polyethersulfone nanocomposite membrane, *Chin. J. Polym. Sci.*, 2018, **36**, 49–57, DOI: 10.1007/s10118-018-2004-3.

39 C. H. Chang, H. H. Lee and C. H. Lee, Substrate properties modulate cell membrane roughness by way of actin filaments, *Sci. Rep.*, 2017, **7**, 9068, DOI: 10.1038/s41598-017-09618-y.

40 R. Mukherjee, P. Bhunia and S. De, Impact of graphene oxide on removal of heavy metals using mixed matrix membrane, *Chem. Eng. J.*, 2016, **292**, 284–297, DOI: 10.1016/j.cej.2016.02.015.

41 M. Nadour, F. Boukraa, A. Ouradi and A. Benaboura, Effects of methylcellulose on the properties and morphology of polysulfone membranes prepared by phase inversion, *Mater. Res.*, 2017, **20**, 339–348, DOI: 10.1590/1980-5373-MR-2016-0544.

42 A. M. Nasir, P. S. Goh and A. F. Ismail, Highly adsorptive polysulfone/hydrous iron-nickel-manganese (PSF/HINM) nanocomposite hollow fiber membrane for synergistic arsenic removal, *Separ. Purif. Technol.*, 2019, **213**, 162–175, DOI: 10.1016/j.seppur.2018.12.040.

43 M. R. Adam, N. M. Salleh, M. H. D. Othman, T. Matsuura, M. H. Ali and M. H. Puteh, *et al.*, The adsorptive removal of chromium (VI) in aqueous solution by novel natural zeolite based hollow fibre ceramic membrane, *J. Environ. Manage.*, 2018, **224**, 252–262, DOI: 10.1016/j.jenvman.2018.07.043.

44 S. Mokhtari, A. Rahimpour, A. A. Shamsabadi, S. Habibzadeh and M. Soroush, Enhancing performance and surface antifouling properties of polysulfone ultrafiltration membranes with salicylate-alumoxane nanoparticles, *Appl. Surf. Sci.*, 2017, **393**, 93–102, DOI: 10.1016/j.apsusc.2016.10.005.

45 J. H. Zuo, P. Cheng, X. F. Chen, X. Yan, Y. J. Guo and W. Z. Lang, Ultrahigh flux of polydopamine-coated PVDF membranes quenched in air via thermally induced phase separation for oil/water emulsion separation, *Separ. Purif. Technol.*, 2018, **192**, 348–359, DOI: 10.1016/j.seppur.2017.10.027.

46 Q. Zhao, R. Xie, F. Luo, Y. Faraj, Z. Liu and X. J. Ju, *et al.*, Preparation of high strength poly(vinylidene fluoride) porous membranes with cellular structure via vapor-induced phase separation, *J. Membr. Sci.*, 2018, **549**, 151–164, DOI: 10.1016/j.memsci.2017.10.068.

47 M. Lucas, S. Schlüter, H. J. Vogel and D. Vetterlein, Roots compact the surrounding soil depending on the structures they encounter, *Sci. Rep.*, 2019, **9**, 16236, DOI: 10.1038/s41598-019-52665-w.

48 K. Wang, S. Wu, Y. Huang, R. Wen, Y. Chen and D. Zhou, *et al.*, Increasing the compact density and its consistency in the cross-section for enhancing the anti-corrosion and mechanical properties of micro-arc oxidation coatings, *J. Mater. Res. Technol.*, 2022, **21**, 1344–1352, DOI: 10.1016/j.jmrt.2022.09.110.

49 H. Pöllmann and S. Auer, Cr^{6+}-containing phases in the system CaO – Al_2O_3 – CrO_4^{2-} – H_2O at 23 °C, *J. Solid State Chem.*, 2012, **185**, 82–88, DOI: 10.1016/j.jssc.2011.10.022.

50 D. Nie, R. Ma, Y. Zhang, W. Wang, G. Nie, G. Liu, W. Liu and D. Zou, Efficient removal of Cr(VI) from wastewater by composite adsorptive membrane modified with polyethyleneimine (PEI), *Separ. Purif. Technol.*, 2024, **346**, 127410, DOI: 10.1016/j.seppur.2024.127410.

51 F. Yang, Y. Jiang, M. Dai, X. Hou and C. Peng, Active biochar-supported iron oxides for Cr(VI) removal from groundwater: Kinetics, stability and the key role of FeO in electron-transfer mechanism, *J. Hazard. Mater.*, 2022, **424**, 127542, DOI: 10.1016/j.jhazmat.2021.127542.

52 S. Basu, G. Ghosh and S. Saha, Adsorption characteristics of phosphoric acid induced activation of bio-carbon: Equilibrium, kinetics, thermodynamics and batch adsorber design, *Process Saf. Environ. Protect.*, 2018, **117**, 125–142, DOI: 10.1016/j.psep.2018.04.015.

53 A. Senol, İ. M. Hasdemir, B. Hasdemir and İ. Kurdaş, Adsorptive removal of biophenols from olive mill wastewaters (OMW) by activated carbon: mass transfer, equilibrium and kinetic studies, *Asia-Pac. J. Chem. Eng.*, 2017, **12**, 128–146, DOI: 10.1002/apj.2060.

54 G. T. El-Bassyouni, S. H. Kenawy, R. S. Hassan, M. Mabrouk and E. M. A. Hamzawy, Removal of 137Cs and 152 + 154Eu using hydroxyapatite prepared from mussel shells, *Interceram*, 2019, **68**, 34–41, DOI: 10.1007/s42411-019-0049-0.

55 M. M. Koli and S. P. Singh, Surface-modified ultrafiltration and nanofiltration membranes for the selective removal of heavy metals and inorganic groundwater contaminants: a review, *Environ. Sci.: Water Res. Technol.*, 2023, **9**, 2803–2829, DOI: 10.1039/D3EW00266G.

56 B. Petrovic, M. Gorbounov and S. M. Soltani, Impact of surface functional groups and their introduction methods on the mechanisms of CO_2 adsorption on porous carbonaceous adsorbents, *Carbon Capture Sci. Technol.*, 2022, **3**, 100045, DOI: 10.1016/j.ccst.2022.100045.

57 Y. Fang, Q. Guan, M. Tang, X. Zhang, X. Wu and H. Zeng, *et al.*, A thermally regenerable cationic MOF adsorption material for sustainable and selective removal of hexavalent

chromium from water, *ACS ES&T Eng.*, 2024, **4**, 639–649, DOI: **10.1021/acsestengg.3c00417**.

58 A. Bermejo-López, B. Pereda-Ayo, J. A. González-Marcos and J. R. González-Velasco, Mechanism of the CO_2 storage and in situ hydrogenation to CH_4. Temperature and adsorbent loading effects over Ru-CaO/Al_2O_3 and Ru-Na_2CO_3/Al_2O_3 catalysts, *Appl. Catal., B*, 2019, **256**, 117845, DOI: **10.1016/j.apcatb.2019.117845**.